Supplementary Materials for:

"A composite rupture model for the great 1950 Assam earthquake across the cusp of the East Himalayan Syntaxis", A. Coudurier-Curveur *et al.*

Correspondence to acoudurierc@ntu.edu.sg

The supplementary materials include:

Appendix A. Methods

Appendix B. Notes

Appendix C. References

Appendix D. Figures S1 to S15

Appendix E. Tables S5 and S6

Appendix F. Author contributions

Additional supplementary dataset and tables:

Assam_Landslide_Scars_mapping.kmz file (Google Earth format)

Table S1 (Excel format)

Table S2 (Excel format)

Table S3 (Excel format)

Table S4 (Excel format)

Appendix A. Methods

A0. Landslides and debris flows mapping

From the satellite imagery available in Google Earth, one can assess the longevity of the present-day scars we mapped. Over more than 35 years (the oldest images dating back to 1984), most of the scars have been kept active and visible on all image records (Fig. S1): some scars show enlargement with time, while a significant, larger number of scars has partially recovered vegetation despite the high rainfall in the area. A few of the smallest scars have, indeed, developed over the last ≈ 35 years, but no large one formed over that period. While our observations only go back to 1984, we assume that this landslide evolution trend is representative of the previous 35 years (as supported by Jain *et al.*, 2013). This implies that post-1950 monsoon rainfalls are a second order forcing on the rejuvenation of the scars and that the severe ground shaking from the 1950 Assam earthquake was the primary forcing factor in the formation of these landslides, particularly for the largest ones.

Gigantic debris flows, whose deposits contain logs of wood and large boulders (Poddar, 1950), appear to have reached down to ≈ 40 km into the Assam Plain, west and south of the range-fronts (Fig. 2). They probably account for the surface roughness of the Cartosat DEM. Today, northeast of Sadiya, for instance, the Dibang River now incises ≈ 3 m into the 1950 deposits, exposing layers densely filled with large tree-trunk fragments (Figures 2 and S3). A few kilometres east of Tezu, beheaded trunks, with stump faces incrusted with pebbles, still stand above modern gravel in the bed of a Lohit River tributary, in keeping with Kingdon-Ward's (1953b) descriptions at the time (Note S3 and Fig. S3).

A1. Topographic profile surveys

In the field, we used Total-Station leveling and GPS RTK (Real Time Kinematic positioning), with horizontal and vertical precisions of 5 and 10 cm, respectively, to survey the fluvial terraces and scarps geomorphology. Topographic data were later processed using Matlab software (Figures 5 and 6 and Supplementary Figures S10 and 11).

A2. Shallow fault dip estimates

To constrain fault dip angles at Wakro (Fig. S10) and Pasighat (Fig. S11), we applied the "3-point method" to data from 3 independent sources:

1/ We first use the 3 GPS locations of the emergent thrusts at the steepest parts of the 3 co-referenced surface-scarp profiles. South of Wakro, this yields a Mishmi Thrust plane striking N15°E, and dipping 14° to the east, locally. At Pasighat, the same approach yields less precise results because the spacing and elevation differences of the 3 profiles are much smaller. Nevertheless, it is clear that the Main Himalayan Frontal Thrust, whose local strike is N20°E has a much shallower northwest emergent dip ($\approx 2°$).

2/ Using a global elevation dataset and the GeolMapDataExtractor (GMDE v.5.6) software (Allmendinger and Judge, 2013) yields consistent results (13° and 1.5° for the MT and MFT, respectively).

3/ Integrating our mapped fault trace and the local Pleiades Digital Elevation Model (CNES/ Spot Image) into the Petrel E&P software also yields compatible results (12° and 0.24° for the MT and MFT, respectively). The Pleiades Digital Elevation Models were computed from Pleiades satellite images tri-stereo-pairs, using the Geomatica software

(PCI Geomatics), reaching vertical and horizontal resolutions of 5 and 1 m, respectively. Automatic tie point extraction was performed. Epipolar images and DEM were generated and merged, yielding geocoded DEMs.

A3. Characterizing average fault plane dips across the Syntaxis with Petrel E&P software

We used Petrel E&P to calculate planar surfaces (i.e., polynomial regressions of degree 1) fitting both the 1950 surface fault traces of the MT and MFT, and the clouds of relocated aftershock hypocenters beneath the corresponding mountain ranges (Fig.3). We tested two scenarios for each thrust, as summarized in the following table and shown on Fig. S14:

	"Free"	"Forced"
MT	10°	25° *Fits largest aftershock M5.5*
MFT	13° *Happens to fit largest aftershock M6.3*	7° *Fits 2nd largest aftershock M5.9*

The numbers correspond to the average MT and MFT fault-plane dips. "Free" numbers are for regression scenarios not forced to fit one specific aftershock. On Fig. S14d, shallow and steeply dipping fault planes were extended and connected to provide a visual representation of the 1950 earthquake rupture planes across the Syntaxis.

A4. In-situ produced cosmogenic ^{10}Be dating of terraces

We used cosmogenic ^{10}Be to constrain the duration of exposition of quartz-rich rocks to cosmic rays, and hence to measure the time since they were emplaced at or near the surface. This technique provides the age of abandonment of fluvial terraces or fans, which are passive geomorphic markers of fault offsets.

Near Wakro, three terrace surfaces (Wakro, Kamlang, and South Kamlang) were sampled for ^{10}Be exposure age dating (Fig. 5, Table S5). Samples were collected from boulders well embedded in still perfectly stable, un-cracked, and flat terrace deposits. Because erosion and inheritance are limiting factors to assess surface exposure ages, depth profiling is required to model the exponential decrease of cosmogenic isotopes as a function of depth. We thus sampled a 2 m-deep road cut across the Wakro fan surface (DP, Fig. 5, Table S5). At Pasighat, we could only sample the surface of T2 (Fig. 6).

The samples were crushed, sieved, and cleaned to isolate the quartz fraction. The quartz was purified by three progressive HF/HNO_3 leaches, etching the exterior portion of the crystals in order to remove atmospheric ^{10}Be and ^{26}Al that could have been adsorbed on the mineral surfaces (Brown *et al.*, 1991; Gosse and Phillips, 2001; Kohl and Nishiizumi, 1992). Acid-resistant and mafic minerals were removed from the residue leach by heavy liquid and/or magnetic separation. About 250 mg of ^{9}Be carrier was added to the purified quartz that was then dissolved in HF. Total Be was measured by ICP-MS. Nuclides were chemically isolated using ion exchange columns. After precipitation, $Be(OH)_2$ was heated at 750°C to obtain BeO. The $^{10}Be/^{9}Be$ ratios were measured using the ASTER Accelerator Mass Spectrometer at CEREGE, Aix-en-Provence, France and at the AMS facility at University of Cologne, Germany. Finally, the ratios were converted to ^{10}Be

nuclide concentrations using the measured total Be concentration prior to chemical separation (Table S5). We used the CRONUS 2.3 calculator (Balko *et al.*, 2008) to calculate the local ^{10}Be production rate at our sites. Near Wakro, the fit to the depth profile concentrations and the lowest concentrated sample on the young surface of the Kamlang terrace concur to imply a low value of inheritance (630 at/g). All surface ages, assuming no erosion and using the Lal (*1991*) / Stone (*2000*) time-dependent scaling scheme (Table S5), were calculated with this inheritance value, which, for most samples, represents a correction of less than 10%.

Appendix B. Notes

Note S1.

a. "The flanks of the mountains were mutilated and torn asunder, the wounds gleaming white as snow against the prevailing green of summer." Kingdon-Ward (1953a).

b. "However, a large part of the devastated area will one day be reclothed though it is certain that the scars of the great earthquake will be clearly visible a century hence, and possibly long after that. Some of these will be cliff faces, some will be gullies, but many will be mere mounds of boulders." Kingdon-Ward (1953b).

Note S2.

The valleys most affected were those of the Dibang, Tidding, Lohit rivers, and their tributaries (e.g., Nara): "Damming of the Tidding upstream of a huge landslide formed a 6 km long, 400 m wide lake. The valley was blocked for at least two days upstream of Therongliang, then catastrophically flooded downstream, destroying still standing houses" [Ramachandra Rao, 1953]. Today's remnant lake is smaller (1 km long, 400 m wide), but the upstream sediment fill of the larger, former lake is still visible. In the Subansiri and Dibang, landslides were widespread near the range front and decreased in extent northwards (Ramachandra Rao, 1953). The Brahmaputra remained full of silt throughout the following winter. One long lasting consequence of the earthquake was that the riverbeds in the Assam plain were permanently raised (Kingdom-Ward, 1953b).

Note S3.

Note that none were included in the Centennial catalogue (Engdahl and Villaseñor, 2002) and that modern ISC relocations were all carried out at fixed depth, usually 25 km, but occasionally 15 or 20 km. The iterative interactive method of Wysession *et al.* (1991) includes a Monte Carlo algorithm injecting Gaussian noise to obtain an estimate of a confidence ellipse (for 1950, we use a standard deviation of 3 s). Overall, such relocations and their 90% confidence ellipses are compatible with those obtained by Chen and Molnar (1977).

Note S4.

Many of these escarpments are hidden beneath dense vegetation. The thick, continuous forest cover along the Arunachal Pradesh range-front likely accounts for the fact that co-seismic scarps were not identified and described in the months and years following the earthquake, as well as later. At the time of our study, the lack of bridges between Roing and Mebo prevented access to the 90° bend of the thrust at the Dibang valley outlet. To the west, we could briefly explore only parts of the range-fronts between Ngorlung and the Subansiri. Southeast of Wakro, we only scouted the range-front to about 96.33°E but could not study the area located farther east because of safety issues. Nonetheless, we identified large mountain landslides and sets of uplifted, abandoned terraces suggesting that strong shaking and thrusting in 1950 extended farther southeast, probably as far as Vijaynagar, near the junction of the MT with the northernmost branch of the Sagaing Fault (Figures 1 and 2). Nevertheless, the fine-scale morphology of both of

these western and southeastern-most parts of the mountain fronts is similar to that in between.

Note S5. From Kingdom-Ward, 1953b

"Many trees, hit by flying boulders, snapped off short; but some showed small rocks embedded like bullets in their trunks".

"Approaching the outer range of hills, I expected to find fewer signs of the earthquake. As we reached the Tidding valley, therefore, it came as something of a shock to observe the colossal damage inflicted far worse than anything we had seen previously. The steep hills which flank the gateway to the plains seemed to have been turned inside out."

"The valley was now twice its former width, but it contained nothing but stones piled in vast mounds, with a muddy torrent rushing through the wilderness. It was a graveyard."

Appendix C. References

Allmendinger, R. W. and P. A. Judge. Stratigraphic uncertainty and errors in shortening from balanced sections in the North American Cordillera, *Geological Society of America Bulletin* **125**, no. 9/10, p. 1569-1579 (2013) DOI: 10.1130/B30871.1.

Avouac, J-P., Ayoub, F., Leprince, S., Konca, O., and D. V. Helmberger. The 2005, M_w 7.6 Kashmir earthquake: Sub-pixel correlation of ASTER images and seismic waveforms analysis. *Earth and Planetary Science Letters* **249**, 514-528 (2006) DOI: 10.1016/j.epsl.2006.06.025.

Balco, G., Stone, J. O., Lifton, N. A., and T. J. Dunai. A complete and easily accessible means of calculating surface exposure ages or erosion rates from ^{10}Be and ^{26}Al measurements. *Quaternary geochronology* **3**, 174-195 (2008) DOI: 10.1016/j.quageo.2007.12.001.

Brown, E. T., *et al.* Examination of surface exposure ages of moraines in Arena Valley, Antarctica using in situ produced ^{10}Be and ^{26}Al, *Geochim. Cosmochim. Acta* **55**, 2269–2283 (1991) DOI: 10.1016/0016-7037(91)90103-C.

Chen, W. S. *et al.* Late Holocene paleoseismicity of the southern part of the Chelungpu fault in central Taiwan: Evidence from the Chushan excavation site. *Bull. Seism. Society of America* **97**.1B, 1-13 (2007) DOI: 10.1785/0120050161.

Engdahl, E. R., and A. Villaseñor. Global Seismicity: 1900−1999. International Handbook of Earthquake and Engineering Seismology Part A, pp. 665−690, Academic Press (2002).

Gaudemer, Y., Tapponnier, P. and D.L. Turcotte (1989). River offsets across active strike-slip faults. Annales Tectonicae. Vol. III, n.2: 55-76.

Gosse, J. C. and F. M. Phillips. Terrestrial in situ cosmogenic nuclides: theory and application. *Quaternary Science Reviews* **20**, 1475-1560 (2001) DOI: 10.1016/S0277-3791(00)00171-2.

Huang, M.W., Pan, Y.W., and J.J. Liao. A case of rapid rock riverbed incision in a coseismic uplift reach and its implications, *Geomorphology* **184**, 98-110 (2013) DOI: 10.1016/j.geomorph.2012.11.022.

Jain, S. K., Kumar, V. and Saharia, M. Analysis of rainfall and temperature trends in northeast India, *Int. J. Climatol.* 33: 968-978 (2013) DOI:10.1002/joc.3483.

Kohl, C. P. and K. Nishiizumi. Chemical isolation of quartz for measurement of in-situ-produced cosmogenic nuclides. *Geochimica et Cosmochimica Acta* **56**(9), 3583-3587 (1992) DOI: 10.1016/0016-7037(92)90401-4.

Lal, D. Cosmic ray labeling of erosion surfaces: in situ nuclide production rates and erosion models. *Earth and Planetary Science Letters* **104**, 424-439 (1991) DOI: 10.1016/0012-821X(91)90220-C.

Pathier, E. *et al.* Displacement field and slip distribution of the 2005 Kashmir earthquake from SAR imagery. *Geophysical Research Letters* **33**, L20310 (2006) DOI: 10.1029/2006GL027193.

Stone, J. O. Air pressure and cosmogenic isotopes production. *J. Geophys. Res.* **105** (B10), 23753-23759 (2000) DOI: 10.1029/2000JB900181.

Tandon, A. N. Direction of faulting of the great Assam earthquake of 15 August 1950. *Ind. J. Meteorol. Geophys.* **6**, 61−64, (1955).

Appendix D. Figures

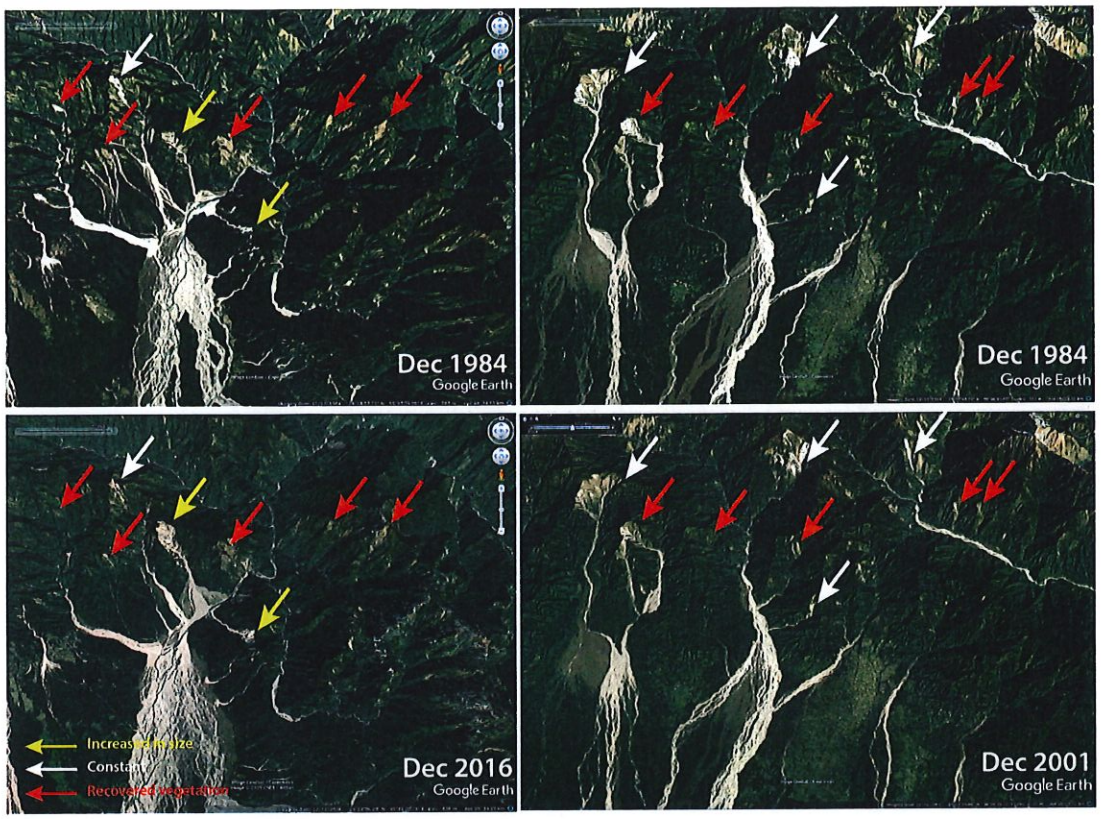

Figure S0. Morphological evolution of landslide scars in the Eastern Himalayan Syntaxis. Left. Evolution of landslide scars in the Dibang Valley over 32 years. Right: Landslide scars evolution in the Mishmi Hills mountain front, near Lohitpur, over 17 years. Yellow, white, and red arrows indicate whether the scars have increased in size, remained constant in size, or have recovered vegetation (i.e., decreased in size), respectively. Note that heavy rainfall, despite common belief, is a then a second order forcing on the rejuvenation process of those scars.

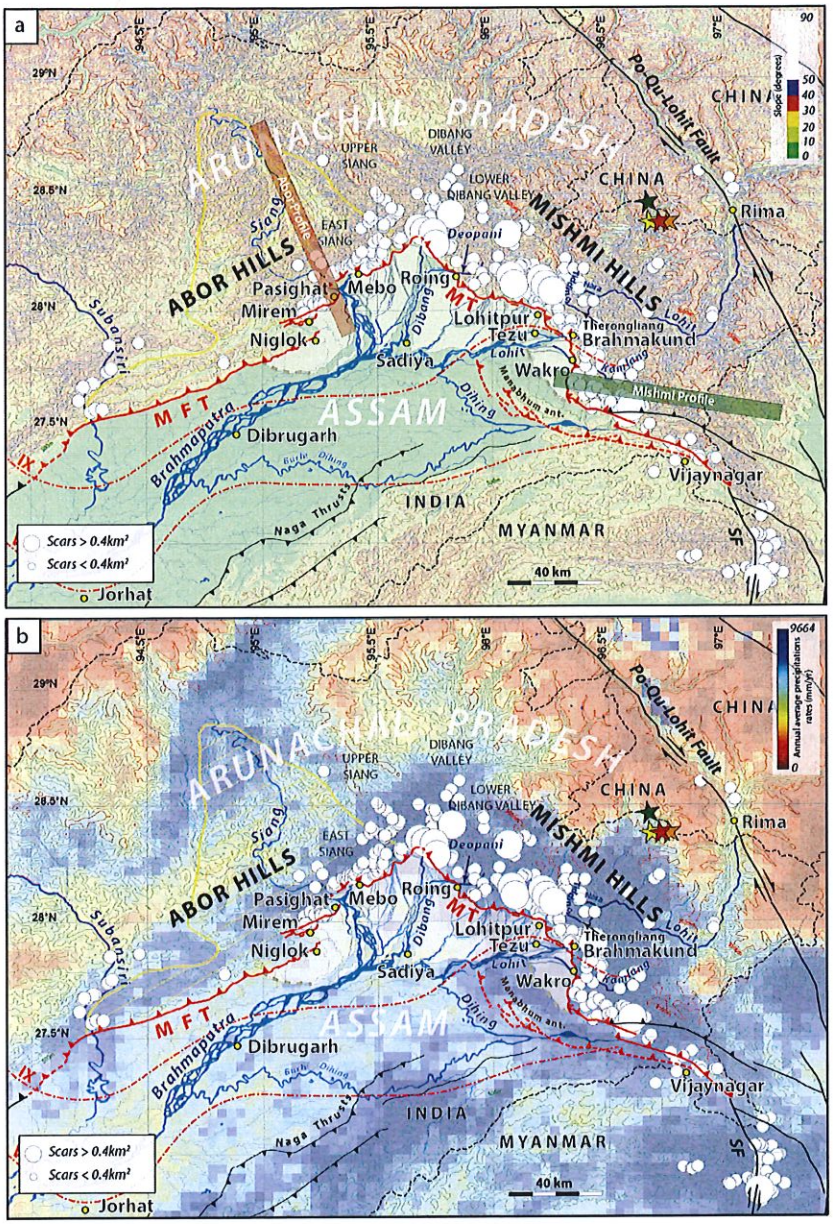

Figure S1. (a) Slope map derived from CARTOSAT C1 topographic data (National Remote Sensing Centre, ISRO, Gov. of India, Hyderabad, India). Symbols and names as in Fig. 2. Green and red boxes are locations of topographic swath profiles shown on Fig. S9 bottom. (b) Rainfall distribution across East Himalayan Syntaxis (averaged annual precipitation rates, for 1998-2009 period, are from TRMM data, Bookhagen, 2008).

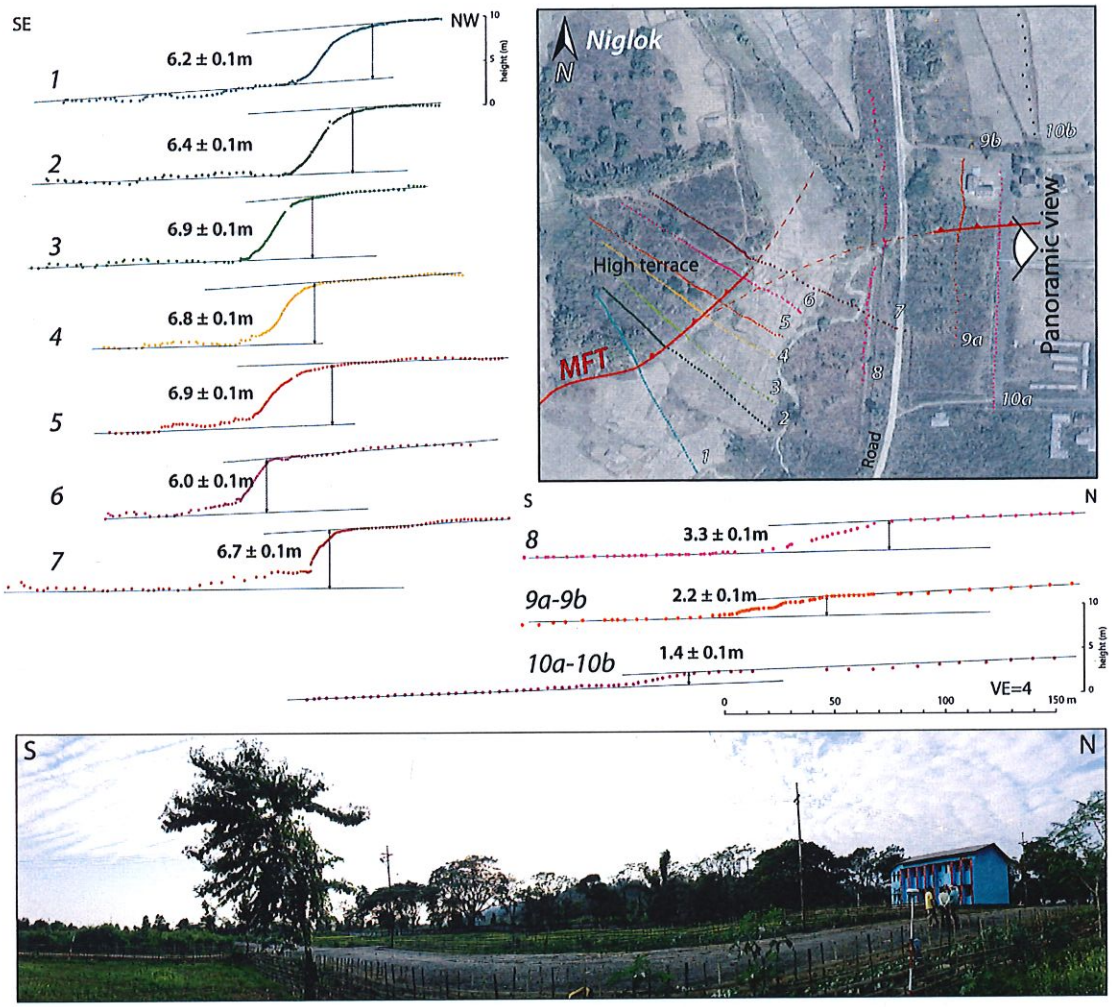

Figure S2. Topographic profiles across Niglok MFT escarpment (eastern Abor Hills front). Note consistent uplift values (6.6 ± 0.4 m) of higher, older terrace to the West, and stepwise decrease of uplift values towards Sille river channel to the East. Scarp height in best-preserved profile west of road (8) is half (3.3 ± 0.1 m) that of higher scarp. Note that both terrace vertical offsets are comparable to those of T1 and T2 at Pasighat (Fig. 6). Bottom. Panoramic view of smoothed topographic scarp across Niglok industrial center.

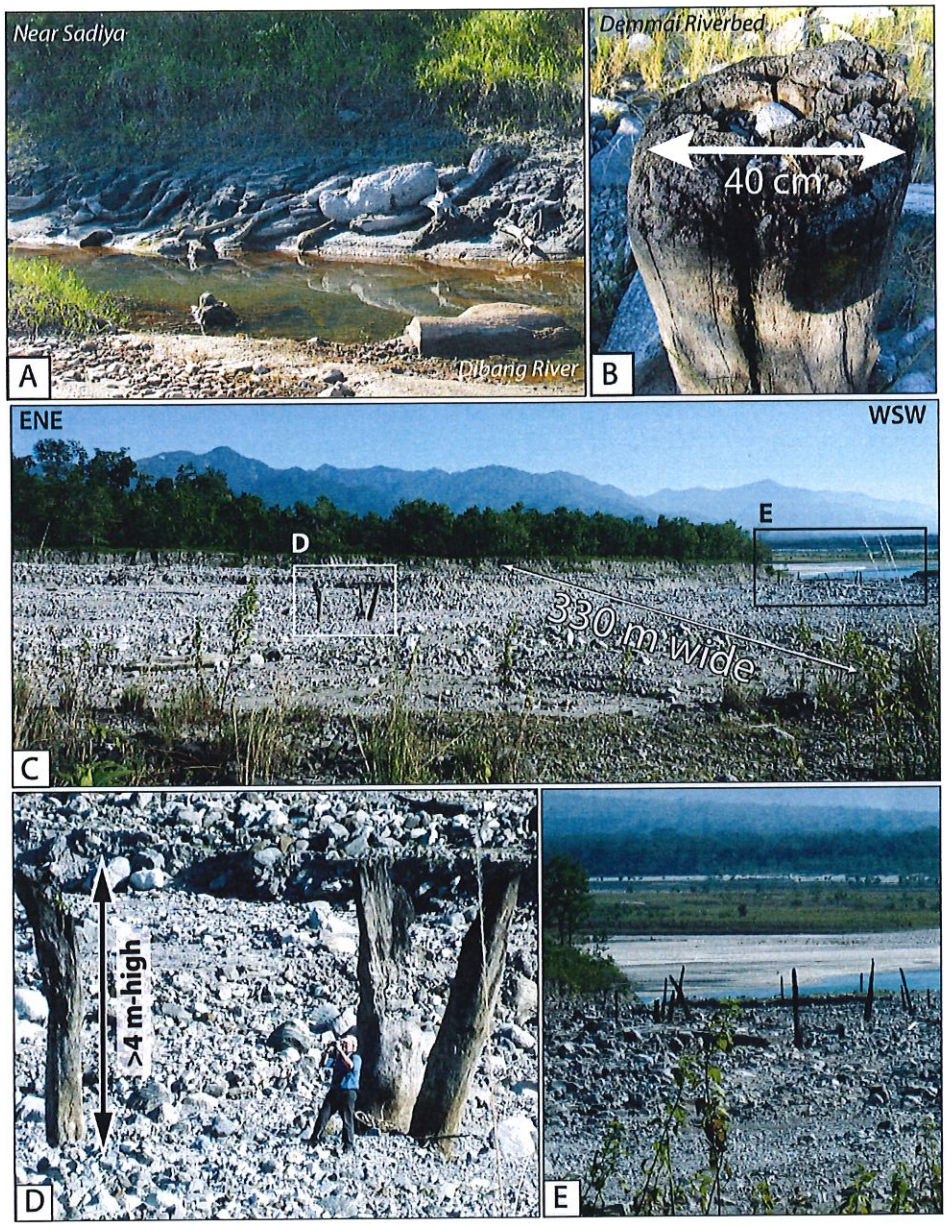

Figure S3. 1950 tree trunk damage. A. Layer of tree logs deposited below modern terrace by post 1950 wash of debris flows along the Dibang River, near Sadiya. B. Tree trunk, still incrusted with pebbles, beheaded by 1950 debris flow in Lohit River tributary (Demmai

River) east of Tezu (see location on Fig. 2). C. Present-day Demmai riverbed exhibiting 4 m-high beheaded tree trunks still standing in the riverbed deposits. Close up in D. and E.

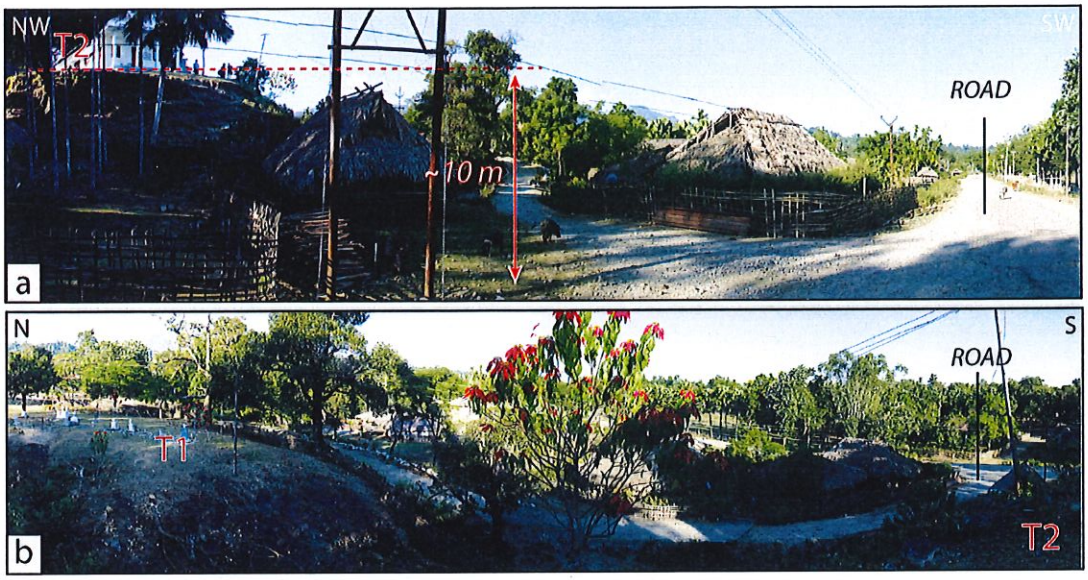

Figure S4. Uplifted, hanging Mirem terraces T1 and T2 along the Abor Hills MFT surface trace. Vertical arrow indicates approximate uplift value of T2 (≈ 10 m). See location on Fig. 2.

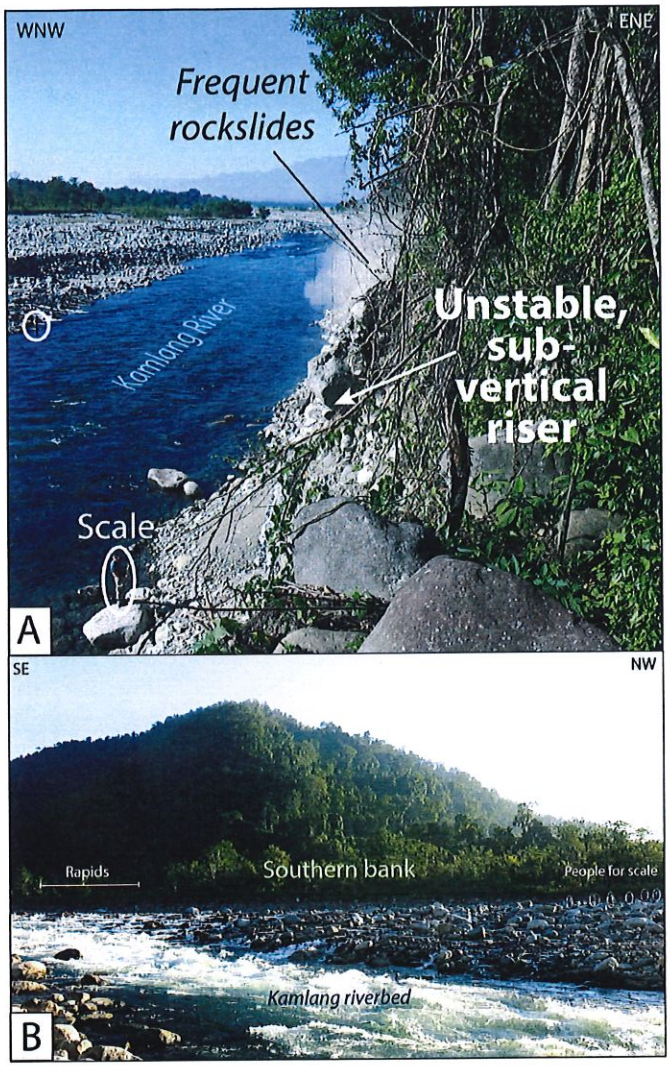

Figure S5. Recent tectonic uplift across Kamlang River valley (Location in Fig. 5A). A. Unstable, ≈ vertical NE terrace riser, exhibiting frequent daily rockslides. B. Vigourous rapids, 100-150 m upstream from the Kamlang scarp, marking receding knick-point southeast of emergent thrust break across riverbed (ESE-WNW view from top of young Kamlang terrace). If that knick-point formed where the 1950 escarpment crossed the river, it would have retreated at an average rate of ≈ 1.85 ± 0.35 m/yr, a plausible value compared to other quantified examples of that process. For further comparison, the 6 m-high co-seismic scarp formed in young and poorly cemented bedrock during the 1999 Chi-Chi earthquake has retreated at the unusually high rate of ≈ 200 m/yr (e.g., Huang et al., 2013).

Table S1 - Landslide scars - Eastern Himalayan Syntaxis						
Rank	a (km^2)Area (k	Rank	a (km^2)Area (k	Rank	a (km^2)Area (k	Rank
1	3.4547	37	0.204191	73	0.1018	109
2	3.2139	38	0.196484	74	0.099658	110
3	1.9134	39	0.193106	75	0.098466	111
4	1.2854	40	0.189488	76	0.097329	112
5	1.046	41	0.18939	77	0.095449	113
6	0.8595	42	0.182536	78	0.094269	114
7	0.8514	43	0.181225	79	0.091886	115
8	0.6836	44	0.178197	80	0.090672	116
9	0.6744	45	0.177005	81	0.089874	117
10	0.5806	46	0.175792	82	0.089197	118
11	0.5689	47	0.17154	83	0.085054	119
12	0.5065	48	0.168468	84	0.08466	120
13	0.4722	49	0.167725	85	0.082332	121
14	0.4301	50	0.165648	86	0.081086	122
15	0.416	51	0.163035	87	0.079173	123
16	0.3874	52	0.16051	88	0.078473	124
17	0.3765	53	0.156324	89	0.077741	125
18	0.3232	54	0.156094	90	0.077697	126
19	0.323	55	0.15229	91	0.077686	127
20	0.3182	56	0.152279	92	0.077468	128
21	0.3008	57	0.149175	93	0.075752	129
22	0.2857	58	0.147502	94	0.075577	130
23	0.2752	59	0.137052	95	0.07491	131
24	0.273	60	0.136899	96	0.074003	132
25	0.2712	61	0.134888	97	0.073861	133
26	0.252	62	0.132243	98	0.073686	134
27	0.2374	63	0.128428	99	0.072964	135
28	0.2341	64	0.120394	100	0.071172	136
29	0.2277	65	0.119508	101	0.069106	137
30	0.2249	66	0.118142	102	0.068789	138
31	0.2247	67	0.116623	103	0.067182	139
32	0.2212	68	0.111605	104	0.066668	140
33	0.2211	69	0.108359	105	0.065531	141
34	0.2169	70	0.106238	106	0.065422	142
35	0.2159	71	0.105276	107	0.065367	143
36	0.208	72	0.102303	108	0.065006	144

a (km²)Area (k	Rank	a (km²)Area (k	Rank	a (km²)Area (k	Rank	a (km²)Area (k
0.063979	145	0.042828	181	0.02736	217	0.019982
0.061541	146	0.042521	182	0.027349	218	0.019654
0.061235	147	0.041877	183	0.027218	219	0.019588
0.06047	148	0.041669	184	0.027076	220	0.019577
0.060394	149	0.041046	185	0.027043	221	0.019556
0.059978	150	0.039996	186	0.027043	222	0.01949
0.05988	151	0.039734	187	0.026956	223	0.019075
0.059596	152	0.039603	188	0.026825	224	0.018976
0.058667	153	0.039155	189	0.026464	225	0.018725
0.058076	154	0.038838	190	0.026191	226	0.018725
0.057814	155	0.037788	191	0.026103	227	0.018441
0.057049	156	0.037581	192	0.026005	228	0.018222
0.056535	157	0.037482	193	0.025786	229	0.018211
0.055912	158	0.037286	194	0.025589	230	0.018145
0.055595	159	0.037089	195	0.02524	231	0.018003
0.054119	160	0.036969	196	0.025043	232	0.017861
0.052971	161	0.036007	197	0.024977	233	0.017741
0.052425	162	0.035045	198	0.024879	234	0.017664
0.05155	163	0.034935	199	0.024835	235	0.017654
0.051507	164	0.034837	200	0.024157	236	0.017326
0.050184	165	0.033307	201	0.024125	237	0.01726
0.049321	166	0.032279	202	0.023349	238	0.016954
0.047768	167	0.032246	203	0.023206	239	0.016866
0.047539	168	0.03182	204	0.02301	240	0.016845
0.046981	169	0.031776	205	0.022496	241	0.016812
0.046774	170	0.031437	206	0.022234	242	0.016582
0.046315	171	0.031405	207	0.022223	243	0.016331
0.045877	172	0.031142	208	0.021436	244	0.016265
0.045855	173	0.030508	209	0.021436	245	0.016156
0.04567	174	0.030257	210	0.021304	246	0.015402
0.045309	175	0.029699	211	0.021294	247	0.015216
0.044948	176	0.029295	212	0.021283	248	0.015183
0.044861	177	0.028847	213	0.020856	249	0.014932
0.044139	178	0.028628	214	0.020758	250	0.014866
0.043527	179	0.028257	215	0.020539	251	0.014702
0.042882	180	0.027907	216	0.020091	252	0.014418

Rank	a (km^2)Area (k	Rank	a (km^2)Area (k	Rank	a (km^2)Area (k	Rank
253	0.01386	289	0.009422	325	0.006296	361
254	0.013729	290	0.009401	326	0.006253	362
255	0.01338	291	0.009182	327	0.006198	363
256	0.013303	292	0.009182	328	0.006187	364
257	0.013259	293	0.008788	329	0.006176	365
258	0.013259	294	0.008701	330	0.005957	366
259	0.013216	295	0.008646	331	0.005706	367
260	0.01315	296	0.008646	332	0.005629	368
261	0.01315	297	0.008635	333	0.005608	369
262	0.013008	298	0.008548	334	0.005553	370
263	0.012702	299	0.008308	335	0.005411	371
264	0.012702	300	0.008242	336	0.005312	372
265	0.012374	301	0.008209	337	0.005236	373
266	0.012363	302	0.008089	338	0.004963	374
267	0.012341	303	0.008078	339	0.004952	375
268	0.012265	304	0.008012	340	0.004766	376
269	0.011904	305	0.007925	341	0.004766	377
270	0.011849	306	0.007892	342	0.004668	378
271	0.011849	307	0.007641	343	0.004646	379
272	0.01174	308	0.007521	344	0.004569	380
273	0.011729	309	0.007422	345	0.004558	381
274	0.011641	310	0.007422	346	0.004558	382
275	0.011357	311	0.007302	347	0.004493	383
276	0.011051	312	0.007193	348	0.004471	384
277	0.010865	313	0.007072	349	0.004438	385
278	0.0108	314	0.007018	350	0.004351	386
279	0.010745	315	0.006821	351	0.004329	387
280	0.010494	316	0.006821	352	0.004296	388
281	0.010286	317	0.006777	353	0.004263	389
282	0.010286	318	0.006755	354	0.004176	390
283	0.010013	319	0.00657	355	0.004143	391
284	0.010002	320	0.006548	356	0.004055	392
285	0.009903	321	0.006537	357	0.00399	393
286	0.009739	322	0.006471	358	0.003891	394
287	0.009663	323	0.006471	359	0.003837	395
288	0.009499	324	0.006395	360	0.003837	396

a (km²)Area (k	Rank	a (km²)Area (k	Rank	a (km²)Area (km²)
0.003826	397	0.001421	433	0.000317
0.00376	398	0.001388	434	0.00024
0.00352	399	0.001301	435	0.00024
0.003509	400	0.001235	436	0.000219
0.003454	401	0.001224	437	0.000208
0.0034	402	0.001213	438	0.000208
0.003345	403	0.001213	439	0.000175
0.003334	404	0.001159	440	0.000164
0.003104	405	0.001115	441	0.000142
0.003093	406	0.001028	442	0.000131
0.003093	407	0.000995	443	0.000131
0.003072	408	0.000951	444	0.00012
0.003028	409	0.000907	445	0.000109
0.002962	410	0.000864	446	0.000087
0.002962	411	0.000853	447	0.000077
0.002929	412	0.000853	448	0.000055
0.002875	413	0.000842	449	0.000033
0.002864	414	0.000831	450	0.000033
0.002842	415	0.000787	451	0.000022
0.002798	416	0.000776		
0.002678	417	0.000743		
0.002602	418	0.000721		
0.002503	419	0.000711		
0.002481	420	0.0007		
0.002459	421	0.000601		
0.002405	422	0.00059		
0.002361	423	0.000481		
0.002	424	0.000481		
0.002	425	0.000459		
0.001957	426	0.000448		
0.001902	427	0.000448		
0.001869	428	0.000437		
0.001662	429	0.000415		
0.001607	430	0.000394		
0.001498	431	0.000372		
0.001465	432	0.000328		

Table S2 - Aftershocks - Fixed Depths- Relocation

DD	MM	JJ	YY	Origin Time	Lat.	Lon.	Depth	Fixed (1) or Floated (0) depth	N0	N1	Sigma	Magnitude
15	AUG	227	1950	14:09:31.1	28.37	96.72	10	1	178	169	2.3	8.7 PAS
15	AUG	227	1950	15:57:52.8	29.55	95.27	20	1	18	17	1.27	
15	AUG	227	1950	16:29:24.2	26.96	97.1	20	1	35	35	3.84	
15	AUG	227	1950	16:50:03.7	28.69	95.77	20	1	28	26	3.71	
15	AUG	227	1950	17:17:01.1	28.72	94.97	20	1	33	30	3.34	
15	AUG	227	1950	18:38:46.0	28.57	95.85	15	1	74	71	2.47	
15	AUG	227	1950	19:58:49.4	28.49	95.96	20	1	28	27	3.24	
15	AUG	227	1950	21:01:33.0	27.43	96.55	20	1	51	50	2.17	
15	AUG	227	1950	21:42:20.2	25.29	92.75	20	1	91	79	3.22	
15	AUG	227	1950	22:30:54.5	28.56	95.64	20	1	19	17	2.83	
15	AUG	227	1950	23:44:44.4	28.72	95.01	20	1	66	63	5.41	
16	AUG	228	1950	05:33:10.3	28.69	96.72	20	1	65	59	3.23	
16	AUG	228	1950	06:42:03.6	28.45	95.63	20	1	90	88	3.29	6.25 PRA
16	AUG	228	1950	11:28:32.0	28.39	95.63	20	1	38	38	2.55	
16	AUG	228	1950	12:38:26.9	27.78	92.27	20	1	26	25	1.68	
16	AUG	228	1950	15:29:29.0	29.03	94.86	20	1	52	50	4.23	5.75 PRA
16	AUG	228	1950	16:36:02.3	28.68	94.89	20	1	37	35	3.22	
16	AUG	228	1950	17:51:35.4	27.42	92.44	20	1	76	74	3.77	
16	AUG	228	1950	19:25:38.6	28.88	95.75	20	1	53	49	2.04	5.50 PRA
16	AUG	228	1950	20:01:41.0	28.18	95.67	20	1	17	15	3.66	
16	AUG	228	1950	20:11:17.2	27.03	97.33	20	1	44	42	3.12	
16	AUG	228	1950	21:44:22.5	29.29	95.48	20	1	35	32	1.98	
16	AUG	228	1950	22:28:55.7	27.91	95.75	20	1	14	14	2.13	
16	AUG	228	1950	23:21:25.7	26.97	96.94	20	1	48	47	2.23	
17	AUG	229	1950	01:54:15.7	28.42	94.81	20	1	76	74	2.38	5.88 PRA
17	AUG	229	1950	03:44:07.8	27.49	94.94	20	1	15	14	3.45	
17	AUG	229	1950	05:29:19.5	30.19	94.75	20	1	61	59	4.69	5.50 PRA
17	AUG	229	1950	08:05:02.5	28.47	95.44	20	1	20	18	3.56	
17	AUG	229	1950	10:30:48.0	26.35	95.77	20	1	29	28	4.42	
17	AUG	229	1950	14:44:01.3	25.86	96.44	20	1	27	25	3	
17	AUG	229	1950	23:56:30.8	27.38	92.56	20	1	20	19	1.22	
18	AUG	230	1950	01:07:53.9	29.18	96.1	20	1	99	97	2.91	7.0 PAS
18	AUG	230	1950	11:20:24.7	29	95.06	20	1	26	23	1.84	
18	AUG	230	1950	16:58:51.9	29.66	96.54	20	1	89	86	2.31	5.88 PRA
18	AUG	230	1950	18:30:07.0	29.01	94.96	20	1	12	10	4.77	
18	AUG	230	1950	22:17:48.1	28.98	95.57	20	1	41	39	2.64	
19	AUG	231	1950	21:20:03.0	28.73	95.65	20	1	27	26	4.3	
20	AUG	232	1950	09:03:40.6	29.67	94.98	20	1	74	69	2.98	5.50 PRA
20	AUG	232	1950	10:37:08.8	27.99	95.14	20	1	17	16	3.82	

21	AUG	233	1950	05:51:33.6	27.3	96.85	20	1	45	42	3.18	
21	AUG	233	1950	18:43:51.4	28.55	94.96	20	1	39	38	3.12	
21	AUG	233	1950	22:55:40.1	28.83	94.24	20	1	43	42	2.3	
22	AUG	234	1950	01:57:26.6	27.2	97.13	20	1	34	29	3.51	
22	AUG	234	1950	02:22:40.5	30.07	95.25	20	1	54	53	3.99	5.50 PRA
22	AUG	234	1950	06:43:15.4	29.19	94.39	20	1	76	74	2.51	5.7 ROM
22	AUG	234	1950	13:22:25.2	27.43	97.11	20	1	75	71	3.38	
22	AUG	234	1950	17:20:11.5	28.5	95.02	20	1	15	14	3.31	
23	AUG	235	1950	03:09:21.4	28.9	95.16	20	1	83	81	2.38	5.75 STR
23	AUG	235	1950	15:34:01.2	27.15	96.82	20	1	36	35	2.07	
23	AUG	235	1950	18:47:00.7	28.47	96.48	20	1	92	89	2.36	6.00 PRA
24	AUG	236	1950	01:27:50.1	28.42	96.63	20	1	48	43	3.38	
25	AUG	237	1950	08:14:08.7	28.5	95.13	20	1	29	28	2.86	
25	AUG	237	1950	13:03:30.0	28.98	95.52	20	1	17	17	2.63	
25	AUG	237	1950	16:57:54.6	28.36	94.9	20	1	15	15	4.21	
26	AUG	238	1950	01:30:02.6	28.51	95.52	20	1	16	15	2.31	
26	AUG	238	1950	06:33:09.7	27	94.92	20	1	58	54	3.14	6.1 STR
27	AUG	239	1950	11:00:04.2	29.27	94.63	20	1	41	41	3.04	
29	AUG	241	1950	09:05:07.3	28.42	94.38	20	1	21	21	3.31	
30	AUG	242	1950	06:24:50.5	29.15	94.99	20	1	12	12	3.38	
31	AUG	243	1950	01:26:26.4	26.73	95.18	20	1	16	15	6.19	
31	AUG	243	1950	19:52:35.4	28.47	95.42	20	1	48	47	2.8	
1	SEP	244	1950	07:12:01.8	29.69	95.43	20	1	45	45	2.59	
1	SEP	244	1950	07:32:51.4	25.93	96.94	20	1	11	10	2.52	
1	SEP	244	1950	23:44:41.7	29.68	95.32	20	1	41	40	3.14	
2	SEP	245	1950	16:14:41.5	29.63	96.73	20	1	86	85	2.34	
3	SEP	246	1950	02:54:58.1	27.76	94.64	20	1	31	31	3.13	
3	SEP	246	1950	23:30:43.8	29.08	95.59	10	1	35	33	1.38	
4	SEP	247	1950	06:19:04.1	28.73	96.37	20	1	46	46	3.2	
4	SEP	247	1950	08:12:35.8	29.8	96.71	10	1	26	25	2.42	
4	SEP	247	1950	22:29:09.1	29.62	96.86	20	1	13	13	2.43	
5	SEP	248	1950	20:18:18.5	29.34	91.76	20	1	21	21	2.85	
8	SEP	251	1950	15:26:29.6	28.2	96.02	20	1	19	19	3.51	
10	SEP	253	1950	10:30:26.1	28.57	95.26	20	1	24	24	2.59	
11	SEP	254	1950	00:18:31.8	28.05	94.81	20	1	40	40	2.67	
11	SEP	254	1950	09:39:52.4	28.62	94.02	20	1	46	44	2.68	
12	SEP	255	1950	20:31:45.8	28.51	95.19	20	1	21	21	3.96	
13	SEP	256	1950	11:07:39.2	27.65	94.85	20	1	47	45	3.35	
14	SEP	257	1950	02:31:33.3	28.45	94.85	20	1	18	18	2.74	
17	SEP	260	1950	15:55:58.7	32.24	94.13	20	1	32	32	3.36	
17	SEP	260	1950	21:33:20.9	32.06	94.23	20	1	25	25	2.71	
18	SEP	261	1950	19:06:59.4	33.47	93.87	20	1	20	17	3.85	
25	SEP	268	1950	12:25:22.5	23.78	94.32	20	1	15	15	5.29	
30	SEP	273	1950	07:28:58.1	28.75	94.48	20	1	111	106	2.7	6.25 PRA

3	OCT	276	1950	23:02:01.3	27.77	96.93	20	1	45	45	3.52	
8	OCT	281	1950	04:50:16.4	28.51	94.36	20	1	54	54	2.32	
16	OCT	289	1950	15:42:35.9	28.51	95.3	20	1	35	35	3.24	
30	OCT	303	1950	09:04:55.5	26.36	96.61	20	1	25	25	3.36	
30	OCT	303	1950	23:14:05.9	32.94	95.51	20	1	24	24	4.1	
2	NOV	306	1950	20:17:31.6	30.3	97.25	20	1	40	40	2.34	
16	NOV	320	1950	09:09:02.4	25.78	96.43	20	1	23	23	3.54	
18	NOV	322	1950	00:44:15.5	27.86	95.71	20	1	18	18	4.35	
21	NOV	325	1950	07:10:06.1	28.57	95.96	20	1	25	25	3.26	
3	DEC	337	1950	06:26:56.3	28.75	95.7	20	1	57	57	3.01	
29	DEC	363	1950	22:35:21.5	23.87	91.93	20	1	47	46	3.01	

N0 : Number of stations read

N1 : Number of Stations kept in final location

Sigma : r.m.s. of residuals in final solution (seconds)

Magnitude is from Bulletin, with reporting agency code (PAS: Pasadena; PRA: Prague; ROM: Roma; STR: Strasbourg)

Table S3 - Aftershocks - Floated Depths - Relocation

DD	MM	JJ	YY	Origin Time	Lat.	Lon.	Depth	Fixed (1) or Floated (0) depth	N0	N1	Sigma	Magnitude	PLOT FIG.3
15	AUG	227	1950	15:57:53.5	29.49	95.27	27.1	0	18	17	1.27		
15	AUG	227	1950	16:29:25.0	26.94	97.11	26.1	0	35	35	3.85		
15	AUG	227	1950	19:58:54.6	28.5	96.04	62.6	0	28	28	3.77		MT
15	AUG	227	1950	21:01:35.0	27.44	96.53	34.4	0	51	50	2.17		
15	AUG	227	1950	21:42:20.0	25.29	92.75	18.8	0	79	79	3.22		
16	AUG	228	1950	11:28:29.1	28.37	95.64	2.3	0	38	38	2.52		MT & MFT
16	AUG	228	1950	12:38:31.0	27.85	92.21	35	0	26	25	1.63		
16	AUG	228	1950	16:36:00.0	28.68	94.89	4.3	0	35	35	3.18		MFT
16	AUG	228	1950	19:25:39.5	28.88	95.74	26.3	0	49	49	2.06	5.5 PRA	MT
16	AUG	228	1950	20:01:46.5	28.32	95.58	65	0	15	15	3.63		MFT
16	AUG	228	1950	21:44:26.5	29.28	95.46	53.8	0	32	32	1.93		MFT
16	AUG	228	1950	22:28:58.0	27.9	95.75	39.3	0	14	14	2.12		
17	AUG	229	1950	01:54:14.0	28.41	94.81	7.3	0	75	75	3.54	5.88 PRA	MFT
17	AUG	229	1950	03:44:07.5	27.55	94.93	67.3	0	14	14	3.37		
17	AUG	229	1950	05:29:23.1	30.21	94.73	48.9	0	59	59	4.68	5.50 PRA	
17	AUG	229	1950	08:05:09.6	28.48	95.35	35	0	18	18	3.46		MFT
17	AUG	229	1950	14:44:01.5	25.85	96.44	15	0	25	25	2.99		
17	AUG	229	1950	23:56:31.0	27.38	92.59	33	0	20	19	1.21		
18	AUG	230	1950	16:58:50.3	29.67	96.55	9.3	0	86	86	2.31	5.88 PRA	
18	AUG	230	1950	18:30:05.3	28.61	94.84	15	0	12	12	6.36		MFT
18	AUG	230	1950	22:17:49.3	28.99	95.56	28.6	0	39	39	2.64		MFT
19	AUG	231	1950	21:20:09.1	28.79	95.53	66.9	0	25	25	4.24		MFT
21	AUG	233	1950	05:51:41.5	27.22	96.74	91.9	0	42	42	2.95		
22	AUG	234	1950	02:22:42.3	30.06	95.24	33	0	53	53	3.96	5.50 PRA	
22	AUG	234	1950	17:20:11.1	28.5	95.02	17	0	14	14	3.31		MFT
23	AUG	235	1950	15:34:00.8	27.15	96.83	17	0	35	35	2.06		
24	AUG	236	1950	01:27:46.1	28.41	96.63	15	0	43	43	3.36		MT
25	AUG	237	50	16:57:52.9	28.35	94.91	8.9	0	15	15	4.23		MFT
26	AUG	238	1950	06:33:12.3	26.98	94.91	35	0	54	54	3.15	6.1 STR	
27	AUG	239	1950	11:00:06.9	29.38	94.62	34.7	0	41	39	2		
3	SEP	246	1950	02:54:57.1	27.77	94.64	12.8	0	31	31	3.12		MFT
3	SEP	246	1950	23:30:48.8	29.09	95.57	39.7	0	33	33	1.34		MFT
4	SEP	247	1950	08:12:41.8	29.76	96.69	63.6	0	25	25	2.5		
5	SEP	248	1950	20:18:21.5	29.35	91.75	34	0	21	21	2.81		
10	SEP	253	1950	10:30:24.7	28.48	95.26	16	0	24	23	2.05		MFT
11	SEP	254	1950	00:18:31.0	28.1	94.87	15.5	0	40	38	1.98		MFT
11	SEP	254	1950	09:39:57.4	28.66	93.99	61.7	0	44	44	2.66		
12	SEP	255	1950	20:31:47.1	27.98	95.11	55.2	0	20	20	2.28		MFT
13	SEP	256	1950	11:07:43.6	27.6	94.79	57.7	0	45	45	3.24		
30	SEP	273	1950	07:28:59.0	28.74	94.48	26.5	0	107	106	2.7	6.25	MFT
3	OCT	276	1950	23:02:05.3	27.76	96.86	51	0	45	45	3.58		MT
8	OCT	281	1950	04:50:15.7	28.51	94.37	15.2	0	54	54	2.32		MFT
16	OCT	289	1950	15:42:38.9	28.49	95.27	45.4	0	35	35	3.25		MFT
30	OCT	303	1950	09:04:55.3	26.36	96.61	18.9	0	25	25	3.37		
16	NOV	320	1950	09:09:01.8	25.63	96.45	24.8	0	23	22	2.71		
18	NOV	322	1950	00:44:14.8	27.85	95.73	15.5	0	18	18	4.34		
3	DEC	337	1950	06:26:53.3	28.76	95.71	0.7	0	57	57	2.99		MT
29	DEC	363	1950	22:35:27.9	23.82	91.75	71.2	0	47	46	2.79		

N0 : Number of stations read
N1 : Number of Stations kept in final location
Sigma : r.m.s. of residuals in final solution (seconds)
Magnitude is from Bulletin, with reporting agency code (PAS: Pasadena; PRA: Prague; ROM: Roma; STR: Strasbourg)
MT: MISHMI THRUST ; MFT : MAIN HIMALAYAN FRONTAL THRUST

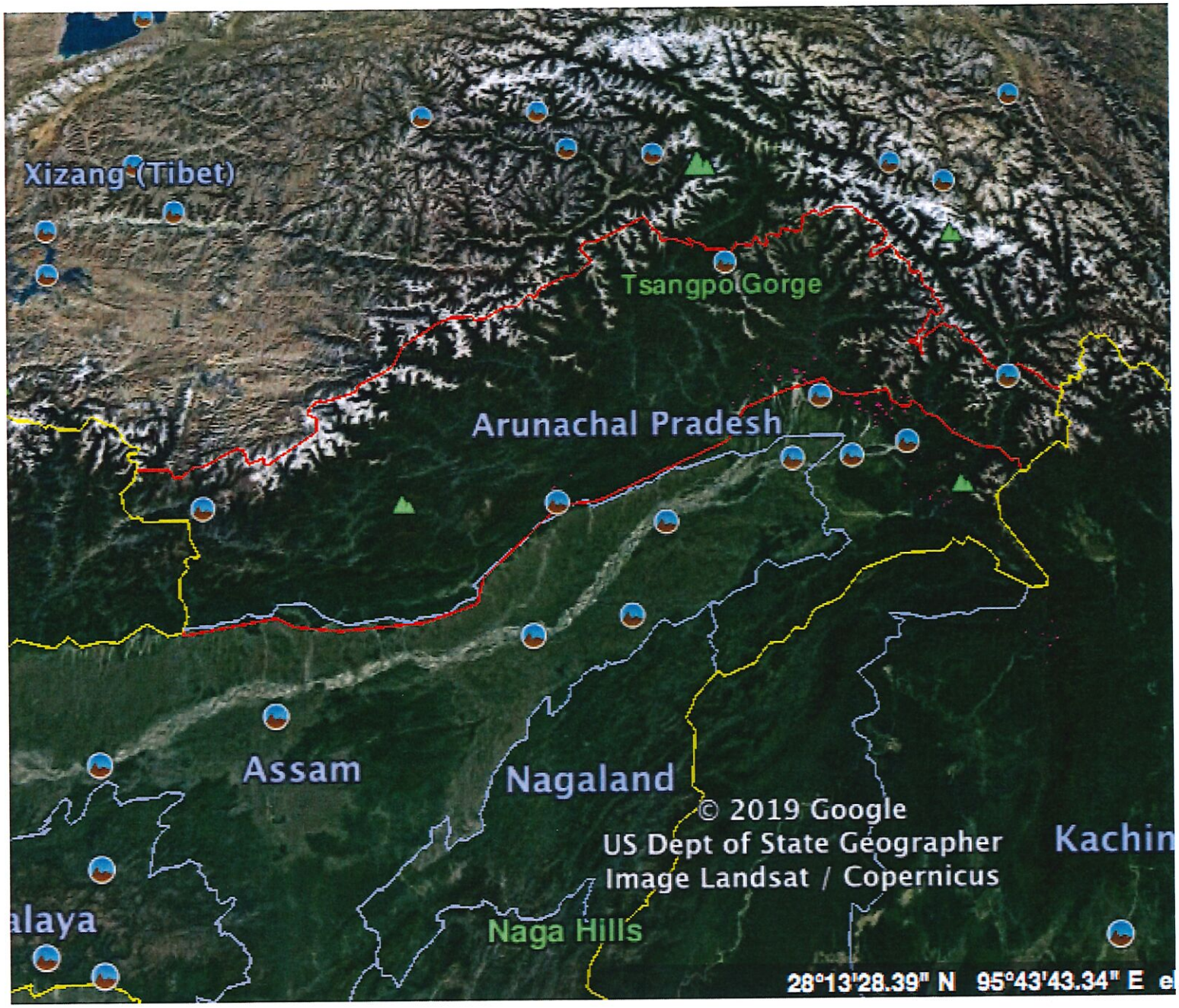
Xizang (Tibet)
Tsangpo Gorge
Arunachal Pradesh
Assam
Nagaland
© 2019 Google
US Dept of State Geographer
Image Landsat / Copernicus
Naga Hills
28°13'28.39" N 95°43'43.34" E

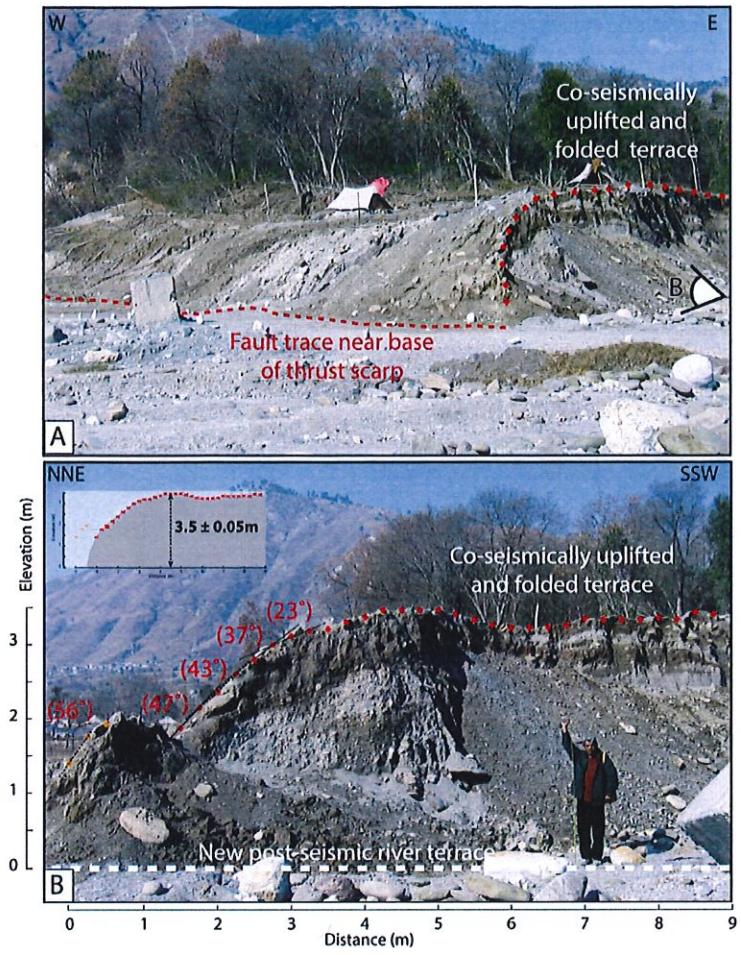

Figure S6. Co-seismic scarp of M_w=7.6 8/10/2005, Muzaffarabad earthquake on Neelum/Kishanganga riverbank, Pakistan (photographs by P. Tapponnier, January 2006). A. View of upward convex, flexural fold scarp bounding youngest, formerly flat, uplifted terrace on river west-bank. Note downward steepening of scarp (56°). White symbol on right side indicates view angle of picture in B. B. Measured co-seismic scarp height and slopes as viewed from the east (Table S4). Prof. A. Kausar holds a 2-m vertical scale. Minimum vertical throw (≈ 3.5 m, top-left inset) is consistent with local sub-pixel ENVISAT SAR and ASTER images correlation (Pathier *et al.,* 2006; Avouac *et al., 2006*).

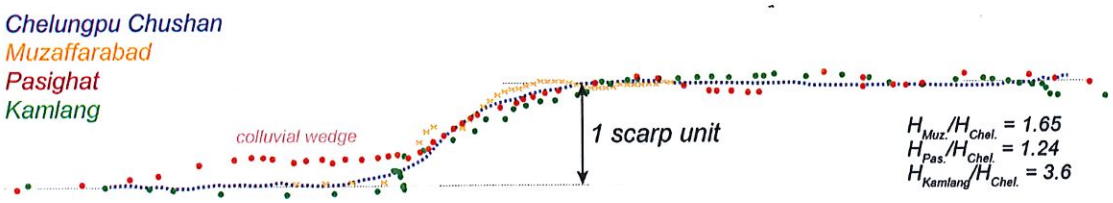

Figure S7. Comparison of co-seismic scarp morphologies associated with recent thrust surface ruptures. Blue dashed line: 1999, M_w=7.6, Chi-Chi earthquake (Taiwan), Chushan site trench (Chen *et al.*, 2007). Orange crosses: 2005, M_w=7.6, Muzaffarabad earthquake (Pakistan), Kishanganga/Neelum river (digitized from field photograph, Fig. S6, Table S4). Green and red dots: 1950, M_w=8.7, Assam earthquake, Kamlang and Pasighat scarps, respectively (Figures 5 and 6). All dimensionless topographic profiles are scaled relative to Chelungpu scarp height. Original scarp heights are: H_{Chel} = 2.1 m; H_{Muz} = 3.46 m; $H_{Pas.}$ = 2.6 m; $H_{Kamlang}$ = 7.6 m.

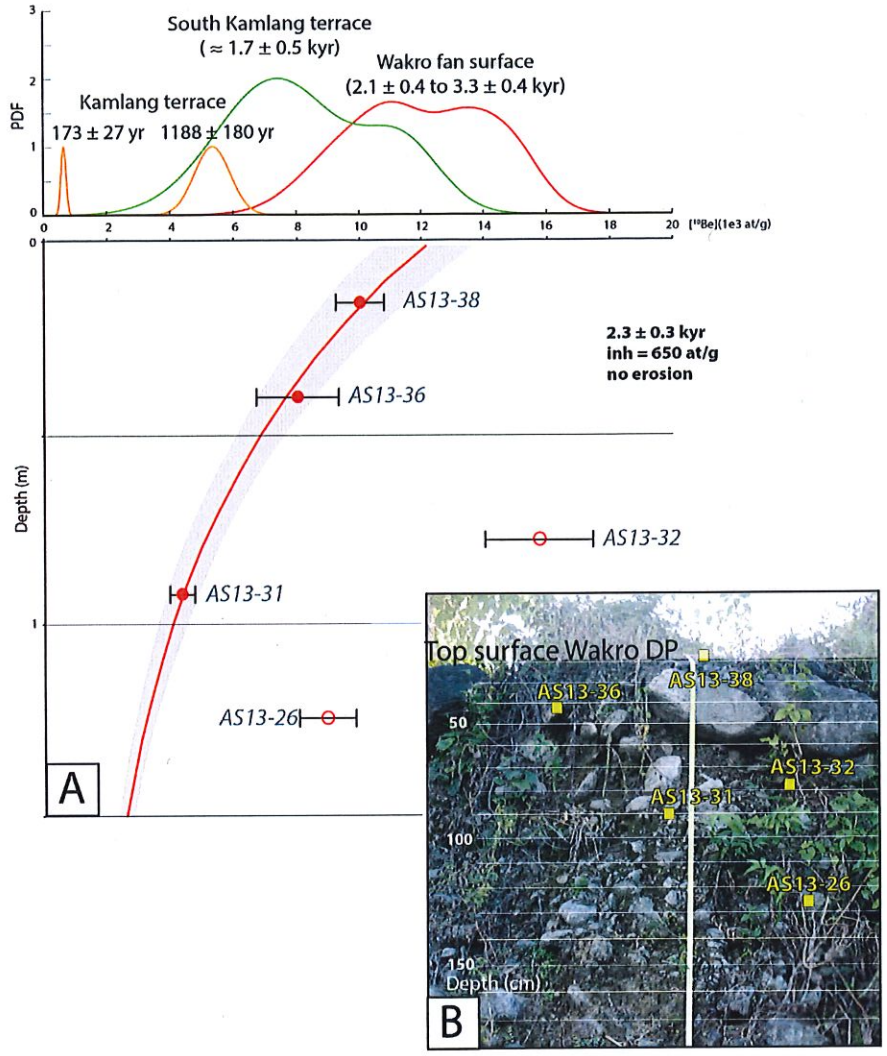

Figure S8. (**A top**) Distribution of ^{10}Be concentrations in surface samples from Kamlang terrace (orange), South Kamlang terrace (green), and Wakro fan surface (red). (**A bottom**). Distribution of ^{10}Be concentrations (as a function of depth) in quartz-rich samples from Wakro fan depth profile (photograph in B). Two samples (78 and 125 cm-depth) that show higher than average concentrations, due to scattered inheritance in sub-surface cobbles, are considered outliers. The best fit for the 3 remaining samples implies an exposure age of 2.3 ± 0.3 kyr, in keeping with surface cobble/block ages. See location and details on Fig. 5 and Table S5.

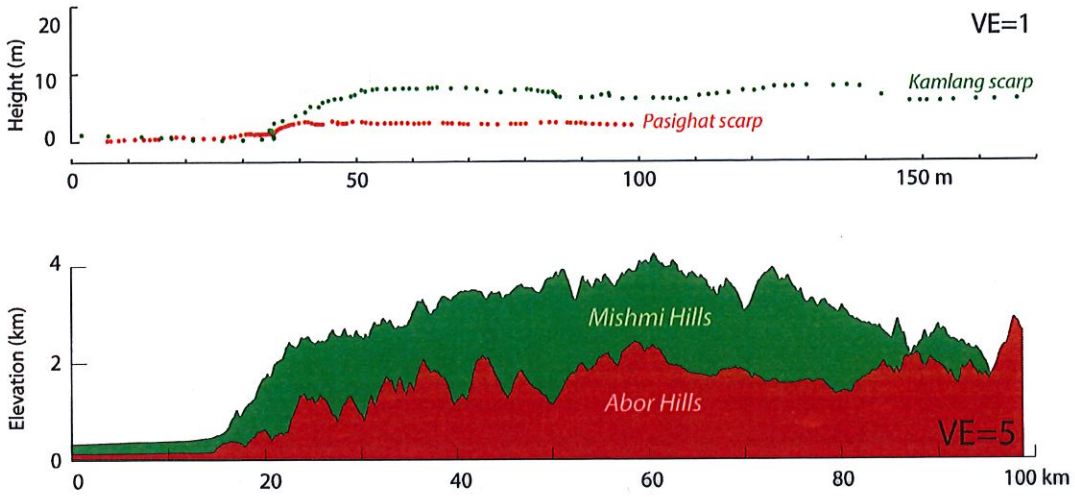

Figure S9. Short and long-term topography across East Himalayan Syntaxis. (Top) Topographic profiles across Kamlang (green) and Pasighat (red) 1950 co-seismic scarps. (Bottom) Topographic profiles across Mishmi (green) and Abor (red) mountain ranges. See locations on Fig. S1a.

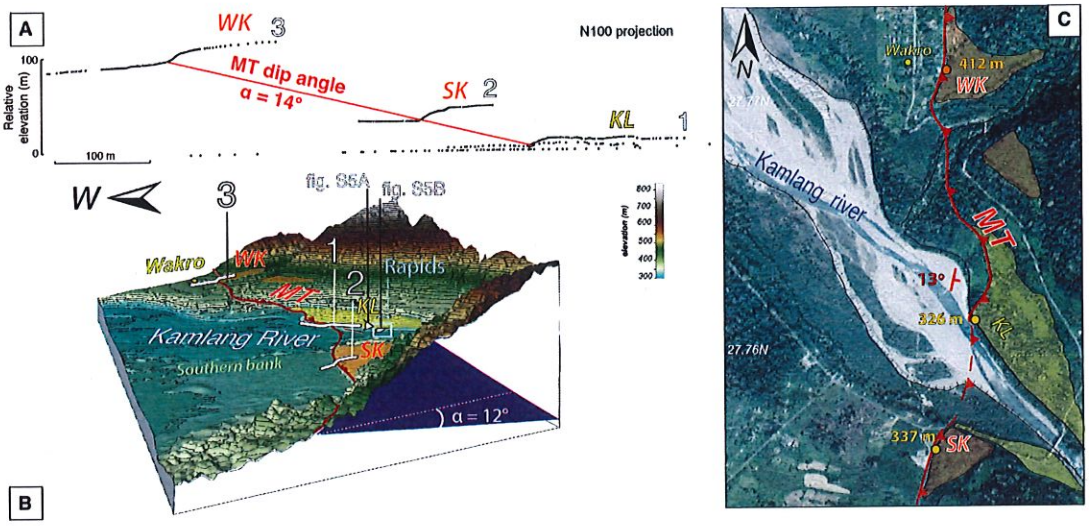

Figure S10. Shallow dip angle of MT at Wakro. A. Co-referenced Total Station topographic profiles (1, 2, 3, location on Fig. 5), ≈ perpendicular to MT scarp, yield thrust plane striking N13°W, dipping 14°E (3-point method, Matlab). B. Trace of MT (red) on 3D Pleiades Digital Elevation Model (CNES/Spot Image) across Kamlang valley implies 12°E dip angle (Petrel E&P software). C. Using the GMDE software (Allmendinger and Judge, 2013), 3 emergent MT point locations (orange dots with corresponding elevations) yield an MT surface dip angle of 13°. See Methods in Appendix A2. Note remarkable consistency (13 ± 1° E).

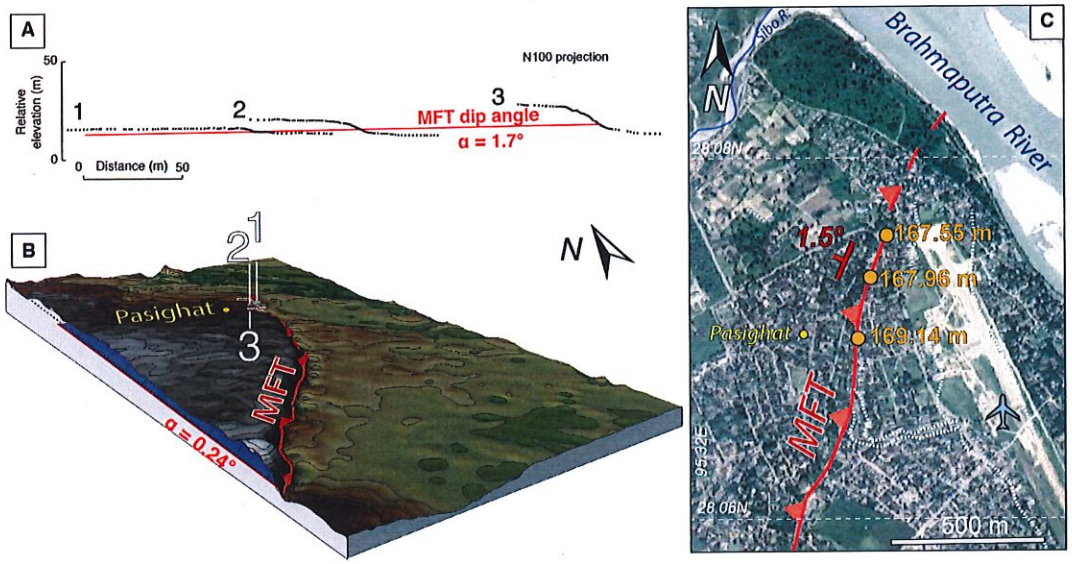

Figure S11. Shallow dip angle of MFT at Pasighat. **A.** Co-referenced Total Station topographic profiles (1, 2, 3, location on Fig. 6), ≈ perpendicular to MFT scarp, yield thrust plane striking N13°E, dipping ≈ 2°W (3-point method, Matlab). **B.** Trace of MFT (red) on 3D Pleiades Digital Elevation Model (CNES/Spot Image) across Brahmaputra valley west bank implies sub-horizontal dip angle (Petrel E&P software). **C.** Using the GMDE software (Allmendinger and Judge, 2013), 3 emergent MT point locations (orange dots with corresponding elevations) yield an MFT surface dip angle of 1.5°. See Methods in Appendix A2. Note that the small elevations differences and the short spacing between data points limit the use and validity of this approach.

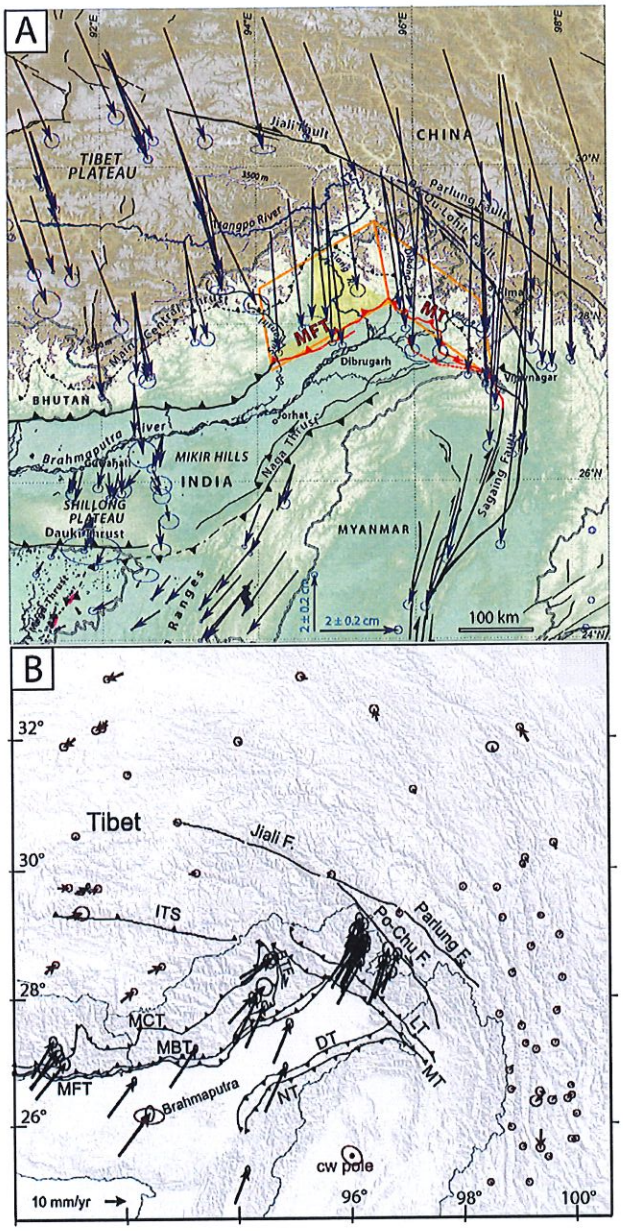

Figure S12. Geodetic data across East Himalayan Syntaxis (EHS). A. GPS displacement vectors (Kreemer *et al.*, 2014) relative to fixed Indian plate. Only GPS data-points located within map area are shown. Background, active faults, 1950 epicenters, 1950 fault model, and other symbols as in Fig. 1. B. Residual velocities (Eurasia-fixed frame) after removal of clockwise rotation around EHS. Extracted from figure 4 in Gupta *et al.* (2015). See that paper for more details.

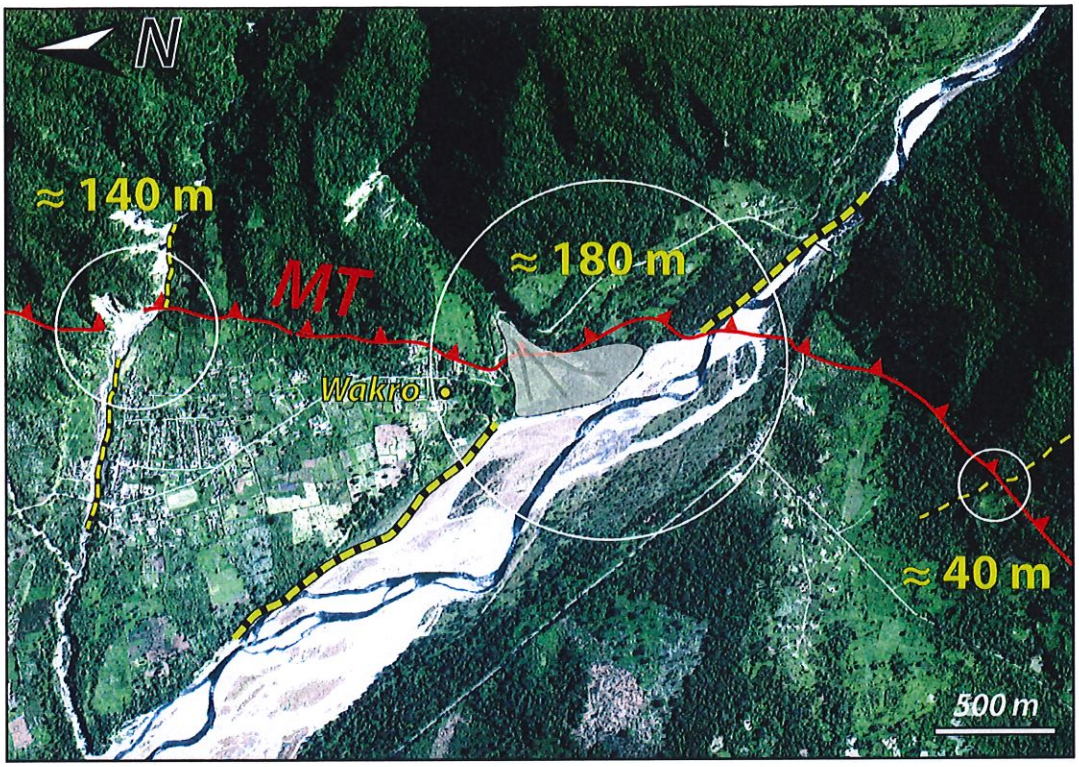

Figure S13. Clear right-lateral drainage offsets observed in the field and on images north and south of Wakro where the MT strikes nearly NS, a direction that maximizes the potential existence of oblique dextral slip (Background: Worldview image). Note relationship between river size and amount of offset (Gaudemer *et al.*, 1989). Incision and offset ages are still unconstrained.

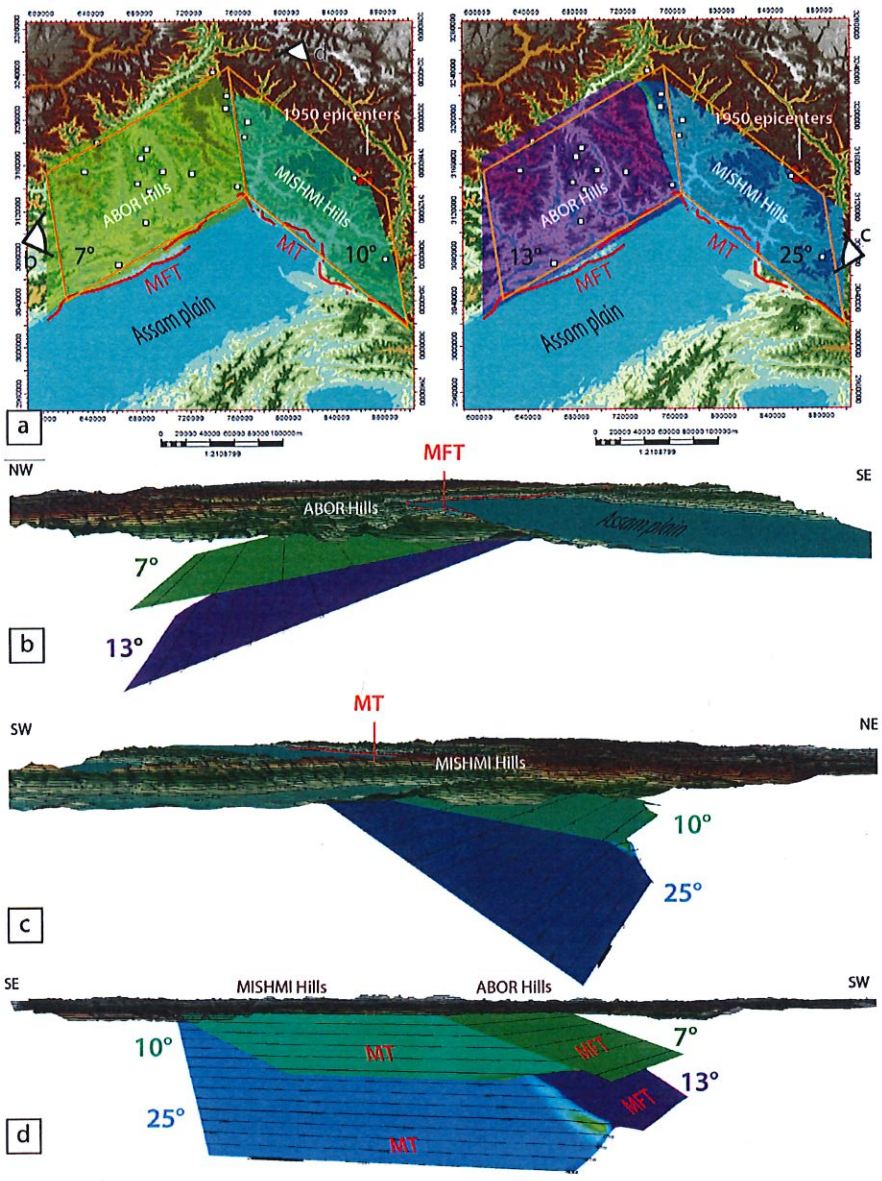

Figure S14. Thrust plane dip angles across East Himalayan Syntaxis cusp, reconstructed using Petrel E&P software (see corresponding table in Appendix A3). (a) Thrust plane horizontal projections. Orange polygons are source geometries from spatial distribution of aftershocks and landslides, as in Fig. 1. (b) 3D view of alternative solutions for MFT (7 and 13°). (c) 3D view of alternative solutions for MT (10 and 25°). (d) Combined MFT and MT thrust planes across Syntaxis.

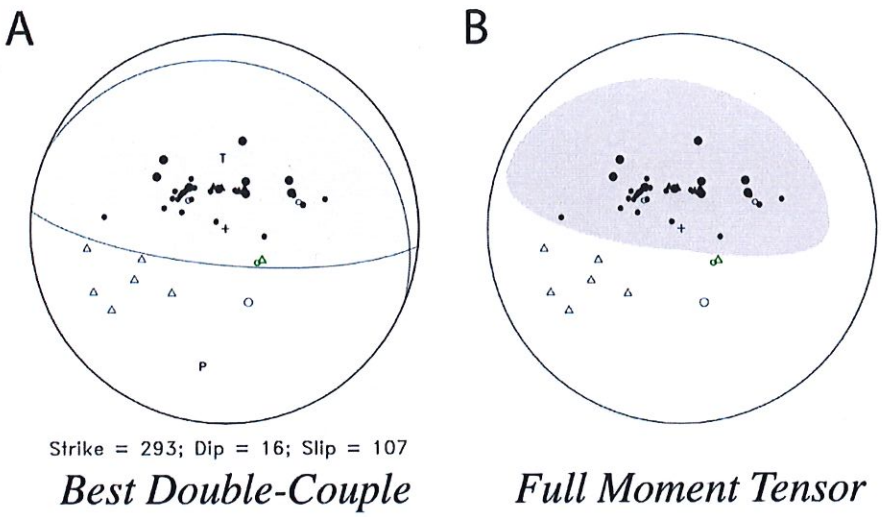

Figure S15. First-motion focal mechanisms for composite solution proposed in this study. A. Best double-couple solution inferred from combination of mechanisms in figure 8 (Bottom right). B. Full, 5-dimensional moment tensor. Note improved fit of arrivals at Riverview and Brisbane (green symbols) by full moment tensor, relative to best double-couple. Polarity symbols as in Fig. 8 top.

Appendix E. Tables

Table S1. List of mapped landslides in Figure 2 (areas in km^2).

Table S2. List of 94 relocated aftershocks of the great, M_w=8.7, 15 August 1950 Assam earthquake (using fixed depth relocation).

Table S3. List of 48 aftershocks of 1950 Assam earthquake relocated using floating depth method, including the 25 selected aftershocks shown in Fig. 3.

Table S4. Ground heights (digitized from scaled field photos, Fig. S6) atop folded and uplifted, pre-seismic, Kishanganga/Neelum river terrace, above new post-seismic terrace across Balakot/Bagh thrust escarpment, NE of Muzaffarabad. 9 m-long profile yields 3.5 m height of 2005 Muzaffarabad, M_w= 7.6 co-seismic throw.

Table S5. Analytical results for cosmogenic isotope dating of quartz-rich samples at Wakro and Pasighat.

Sample name	Location	Type	Thickness (cm)	Rock type	Latitude (°N)	Longitude (°E)	Elevation (m asl)	Depth (cm)	Quartz mass (g)	9Be added (mg)	AMS§ 10Be/9Be (1e-15)	+/- (%)	10Be conc.# (at/g qtz)	+/- (at/g qtz)	Exposure age $ (yrs)	+/- (yrs)
AS13-05*	Wakro North	block 140x330x210	top 5cm	gneiss	27.77121	96.35452	475		13.6196	0.3115	7.781	14.79	9664	1443	**2133**	**395**
AS13-09	Wakro North	block 90x120x150	top 3cm	gneiss	27.77108	96.35439	470		27.3499	0.3073	19.713	6.45	14800	999	**3292**	**384**
AS13-13	Wakro North	cobble 15x20x10	9cm	gneiss	27.76937	96.35296	434		27.2639	0.3086	17.553	6.83	13276	945	**3152**	**376**
AS13-15	Wakro North	cobble 25x13x8	8cm	gneiss	27.76937	96.35296	434		15.9655	0.3092	8.783	9.09	11366	1058	**2676**	**363**
AS13-38	Wakro North DP1	cobble 18x11x10	15cm	gneiss	27.76937	96.35296	434	15	27.6051	0.3086	13.403	7.42	10012	769		
AS13-36*	Wakro North DP1	cobble 20x12x5	12cm	quartzite				40	24.6138	0.1924	15.856	16.15	8025	1306		
AS13-32	Wakro North DP1	cobble 11x13x6	10cm	schist				68	10.2238	0.3097	7.768	10.72	15723	1714		
AS13-31	Wakro North DP1	cobble 13x7x6	6cm	gneiss				92	40.0826	0.3091	8.443	8.81	4350	393		
AS13-26	Wakro North DP1	cobble 25x20x15	10cm	gneiss				125	14.8000	0.3086	6.416	9.91	8939	903		
AS13-41*	Wakro South	block 140x100x35	top 4cm	gneiss	27.75583	96.35454	389		16.9051	0.3112	6.677	25.59	7241	1859	**1636**	**486**
AS13-42*	Wakro South	block 110x60x30	top 6cm	quartzite	27.75584	96.35469	391		9.1069	0.2021	7.474	10.67	11408	1238	**2734**	**405**
AS13-44*	Wakro South	block 120x80x60	top 4cm	quartzite	27.75563	96.35427	393		12.5237	0.2012	9.051	25.98	7550	1967	**1710**	**513**
AS13-50	Wakro Kamlang terrace	block 150x130x60	top 3cm	gneiss	27.75902	96.35679	362		27.1822	0.3092	7.037	10.33	5348	562	**1188**	**180**
AS13-51*	Wakro Kamlang terrace	block 40x30x25	top 4cm	gneiss	27.75973	96.35625	365		46.2511	0.2475	1.753	12.19	647	79	**173**	**27**
AS13-91*	Pasighat	rounded cobble 35x4x17	top 2cm	sandstone	28.07211	95.32925	156		32.3809	0.2990	23.064	5.49	14251	782	**3624**	**376**
AS13-92*	Pasighat	cobble 20x14x11	top 4cm	quartzite	28.07217	95.32922	156		30.6021	0.3043	24.298	5.91	16167	956	**4189**	**443**
AS13-95*	Pasighat	rounded cobble 16x14x8	top 5cm	quartzite	28.07221	95.32938	156		29.9761	0.2995	25.665	4.53	17156	778	**4393**	**432**
AS13-96*	Pasighat	cobble 22x15x12	top 6cm	quartzite	28.07221	95.32940	156		31.6553	0.3012	15.998	6.32	10186	644	**2722**	**290**

* Samples analyzed in the cosmogenic laboratory at Institut de Physique du Globe, University of Strasbourg, France. All other samples analyzed at Institute for Geology and Mineralogy, University of Cologne, Germany.
§ Accelerator mass spectrometry performed on ASTER at CEREGE, Aix-en-Provence, France for sample with (*). Other samples measured at the Cologne, Germany, AMS facility. Ratios are corrected for blank.
# Concentration uncertainties include error on AMS, quartz and standard weighing and error on standard concentration.
$ Exposure age only for surface samples calculate using the Cronus 2.3 exposure age calculator. Shielding and erosion negligible.
*Ages at Wakro calculated with an average inheritance correction of 630 at/g (see text for details), except sample AS13-51.

Table S6.

Shallow dip angles of MT and MFT at Wakro and Pasighat, respectively, using 3 different approaches (see Methods and captions of Figures S10 and S11).

Method	MT dip angle (º)	MFT dip angle (º)
Projection	14	1.7
GeolMapDataExtractor	13	1.5
Petrel	12	0.24

Appendix F. Author contributions

This research was partly supported by the National Research Foundation Singapore and the Singapore Ministry of Education under the Research Centres of Excellence initiative. Access to the field in India and scientific cooperation was made possible through a MoU between CSIR-North-East Institute of Science and Technology (CSIR-NEIST) in Jorhat (India) and EOS (Singapore). PT, ACC, SC, and SB led the study. All authors, save for EO, participated in the fieldwork. PT identified young 1950 surface breaks. ACC analyzed topographic data, designed most of the figures, and contributed to sample processing at IPG Strasbourg. SC and EK identified and mapped landslide scars on satellite imagery. EK processed tri stereo correlation of Pleiades images for the Wakro site. JVDW and EK led the rock sampling, cosmogenic isotope analysis and dating interpretation. EO carried out the seismological research and calculations. SC and SB contributed to field surveys and managed field logistics. ME contributed to field surveys and 3D combination of all datasets using the Petrel software. ÇK contributed to field surveys, rock sampling,

and sample processing at IPG Strasbourg (France). ACC, PT, EO, EK, and JVDW contributed to writing the paper.